fabricated in this letter. To provide an analytical design, the LC equivalent circuit of the main resonator has been precisely calculated. Moreover, Adjusting upper passband is the most noticeable positive point. Considering these features, the proposed filter can be employed in wireless LAN applications.

ACKNOWLEDGMENTS

This work was supported by Semnan University. The measurement result was done by itrc.

ORCID

Shiva Khani http://orcid.org/0000-0002-6703-2029

REFERENCES

[1] Hong JS, Lancaster MJ. *Microstrip Filters for RF/Microwave Applications*. New York: Wiley; 2001.

[2] Wu GC, Wang G, Liang JG, Gao XJ, Zhu L. Miniaturised microstrip dual-band bandpass filter using novel symmetric double-spiral resonators for WLAN application. *Electron Lett.* 2015;51:1177–1178.

[3] Wei XB, Yue GT, Liao JX, Wang P, Xu ZQ, Shi Y. Compact dual-band bandpass filter with ultra-wide upper-stopband. *Electron Lett.* 2013;49:708–709.

[4] Jiang M, Chang LM, Chin A. Design of dual-passband microstrip bandpass filters with multi-spurious suppression. *IEEE Microw Wirel Compon Lett.* 2010;20:199–201.

[5] Kim C, Hyeon Lee T, Shrestha B, Chul Son K. Miniaturized dual-band bandpass filter based on stepped impedance resonators. *Microwave Opt Technol Lett.* 2017;59:1116–1119.

[6] Luo J, Liao C, Zhou H, Xiong X. A novel miniature dual-band bandpass filter based on the first and second resonances for 2.4/5.2 GHz WLAN application. *Microwave Opt Technol Lett.* 2015;57:1143–1146.

[7] Karpuz C, Gorur AK, Sahin E. Dual-mode dual-band microstrip bandpass filter with controllable center frequency. *Microwave Opt Technol Lett.* 2014;57:639–642.

[8] Salehi MR, Abiri E, Noori L. Design of a microstrip dual-band bandpass filter with compact size and tunable resonance frequencies for WLAN applications. *Int J Comput Electr Eng.* 2014;6:248–251.

[9] Khajavi N, Makki SVAD, Majidifar S. Design of high performance microstrip dual-band bandpass filter. *Radioengineering.* 2015;24:32–37.

[10] Song K, Zhang F, Fan Y. Miniaturized dual-band bandpass filter with good frequency selectivity using SIR and DGS. *AEU-Int J Electron Commun.* 2014;68:384–387.

[11] Li Y, Yang HC, Xiao SQ. Design of dual band filter based on a novel DGS structure. *Prog Electromagn Res Lett.* 2013;41:167–174.

[12] Amiri S, Khajavi M. Improvement the design of microwave dual-band BPF by DGS technique. *Microwave Opt Technol Lett.* 2016;58:2133–2137.

[13] Alqaisy M, Chakrabraty C, Ali J, Alhawari AR. A miniature fractal-based dual-mode dual-band microstrip bandpass filter design. *Int J Microw Wirel Technol.* 2015;7:127–133.

[14] Mezaal YS, Eyyuboglu HT, Ali JK. New microstrip bandpass filter designs based on stepped impedance hilbert fractal resonators. *IETE J Res.* 2014;60:257–264.

[15] Zhang S, Zhu L. Synthesis design of dual-band bandpass filters with λ/4 stepped-impedance resonators. *IEEE Trans Microw Theory Tech.* 2013;61:1812–1819.

[16] Cho YH, Yun SW. Design of balanced dual-band bandpass filters using asymmetrical coupled Lines. *IEEE Trans Microw Theory Tech.* 2013;61:2814–2820.

How to cite this article: Khani S, Makki SVAL-D, Mousavi SMH, Danaie M, Rezaei P. Adjustable compact dual-band microstrip bandpass filter using T-shaped resonators. *Microw Opt Technol Lett.* 2017;59:2970–2975. https://doi.org/10.1002/mop.30864

Received: 12 May 2017

DOI: 10.1002/mop.30863

Three-dimensional-printed tapered cavity-backed flush-mountable wideband antenna for UAV

Seongkyu Lee | **Guho Jeoung** | **Jaehoon Choi**

Department of Electronics and Computer Engineering, Hanyang University, 17 Haengdang-Dong, Seongdong-Gu, Seoul 133-791, Korea

Correspondence
Jaehoon Choi, Department of Electronics and Computer Engineering, Hanyang University, 17 Haengdang-Dong, Seongdong-Gu, Seoul 133-791, Korea.
Email: choijh@hanyang.ac.kr

Funding information
Defense Acquisition Program Administration and Agency for Defense Development of Korea

Abstract

A 3D-printed tapered cavity-backed flush-mountable wideband antenna for UAV applications is proposed. The antenna consists of a mono-cone and an exponentially tapered cavity, which are fabricated using 3D printing technology. Performance degradation caused by the

resonance of a conventional cavity is reduced by tapering the cavity. The antenna has the overall dimensions of 224 mm × 224 mm × 34 mm. The measured 10-dB return loss bandwidth of the antenna is 24.4 GHz ranging from 1.3 GHz to 25.7 GHz (180%). The measured radiation pattern has an omnidirectional characteristic over the operating frequency band.

KEYWORDS

3D-printed components, cavity-backed antenna, flush mountable antenna, UAV, UWB antenna

1 | INTRODUCTION

Recently, there has been increasing interest in unmanned aerial vehicle (UAV) technology for a variety of applications, such as monitoring, direction finding, and collecting intelligence.[1] In order to successfully realize such applications, an antenna with an omnidirectional radiation pattern in the horizontal plane and a wide frequency bandwidth is required. In particular, the antenna mounted on a UAV has to have a low profile and be lightweight to meet the aerodynamic requirements and the limits of payload capacity, respectively. To attain these requirements, several low-profile antennas for UAV were proposed.[2–5] Although these antennas have an omnidirectional radiation pattern, have a low profile, and are light weight, their bandwidth is not wide enough for UAV applications. To improve the bandwidth performance, a wideband mono-cone antenna embedded inside the cavity was proposed.[6] However, the bandwidth of the antenna was not wide enough due to the effect of the cavity.

Three-dimensional printing technology is a recent research topic of interest because of its advantages in creating low-cost and lightweight parts, as well as its ease of fabrication. Due to its numerous advantages, many microwave components are being fabricated using 3D printing.[7–9]

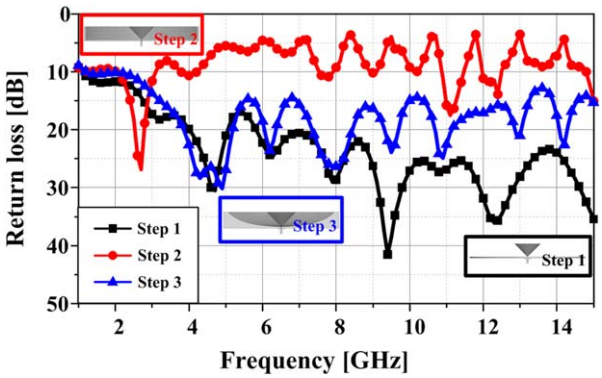

FIGURE 2 Simulated return loss characteristics of each step of the antenna. [Color figure can be viewed at wileyonlinelibrary.com]

Generally, to fabricate a 3D-printed antenna, a conductive material needs to be painted onto the non-conductive structure made by a 3D printer.

In this article, a 3D-printed flush-mountable antenna for UAVs is proposed. All components of the proposed antenna were fabricated using 3D printing technology, and the antenna has a flush-mountable structure in order to meet the requirements for UAV, such as low weight and low air drag. The proposed antenna has an omnidirectional radiation pattern and broad bandwidth. To verify the performance of the proposed antenna, numerical simulations and measurements were performed.

2 | ANTENNA DESIGN

2.1 | Antenna geometry

Figure 1 shows the geometry of the proposed antenna. It has the overall dimensions of 224 mm × 224 mm × 34 mm and consists of a mono-cone and an exponentially tapered cavity. The coaxially fed mono-cone is adopted to achieve wide bandwidth and omnidirectional radiation characteristics. The diameter of the top of the mono-cone is 60 mm, and that of the bottom is 1.5 mm. The exponentially tapered cavity has

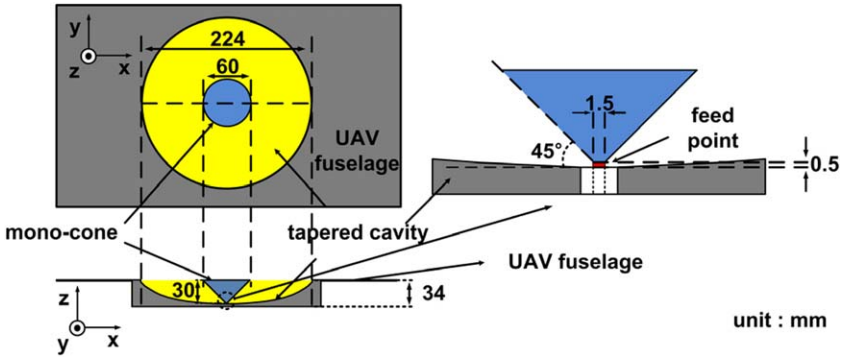

FIGURE 1 Geometry of the proposed antenna. [Color figure can be viewed at wileyonlinelibrary.com]

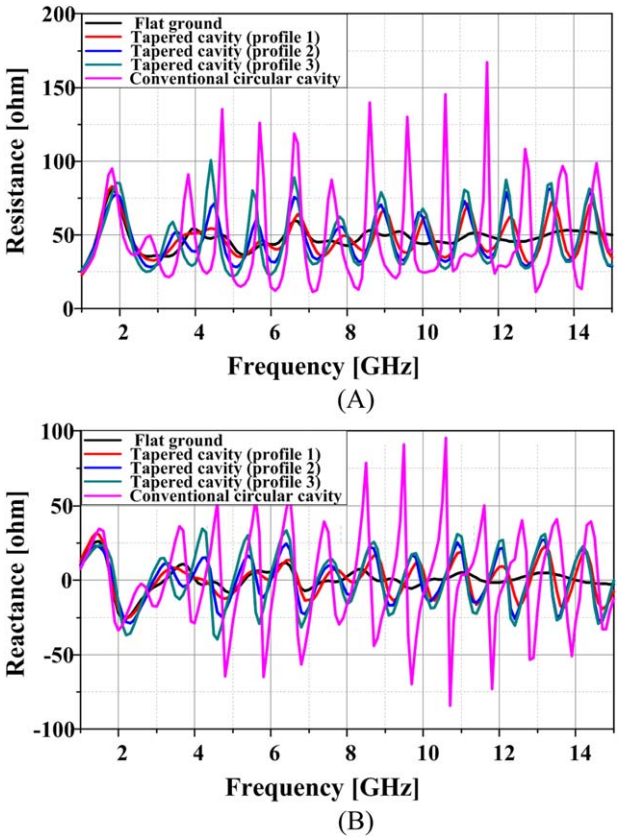

FIGURE 3 Simulated (A) resistance and (B) reactance for the various profiles of the cavity. [Color figure can be viewed at wileyonlinelibrary.com]

TABLE 1 Parameter values of the profile of the bottom of the tapered cavity

Profile no.	A	B
1	1.15E−03	30
2	1.36E−05	70
3	1.85E−08	130

the dimensions of 224 mm × 224 mm × 31 mm, and the profile of the bottom of the tapered cavity is determined by Equation 1, where the center of the bottom of the cavity is located at (0,0,0). The mono-cone is placed at the center of the cavity and the distance between the bottom of the mono-cone and the surface of the cavity is 0.5 mm.

$$z = A(e^{Bx} - 1) \tag{1}$$

2.2 | Design and analysis

The design procedure of the antenna consists of 3 steps, and the Ansoft HFSS is used to design and analyze the performance of the antenna.[10] In step 1, a mono-cone, which has an elevation angle of 45° from the flat circular ground, is designed to achieve a broad bandwidth and monopole-like radiation pattern. The diameter of the flat ground and the height of the mono-cone are set to 230 mm and 30 mm, respectively, in order to establish

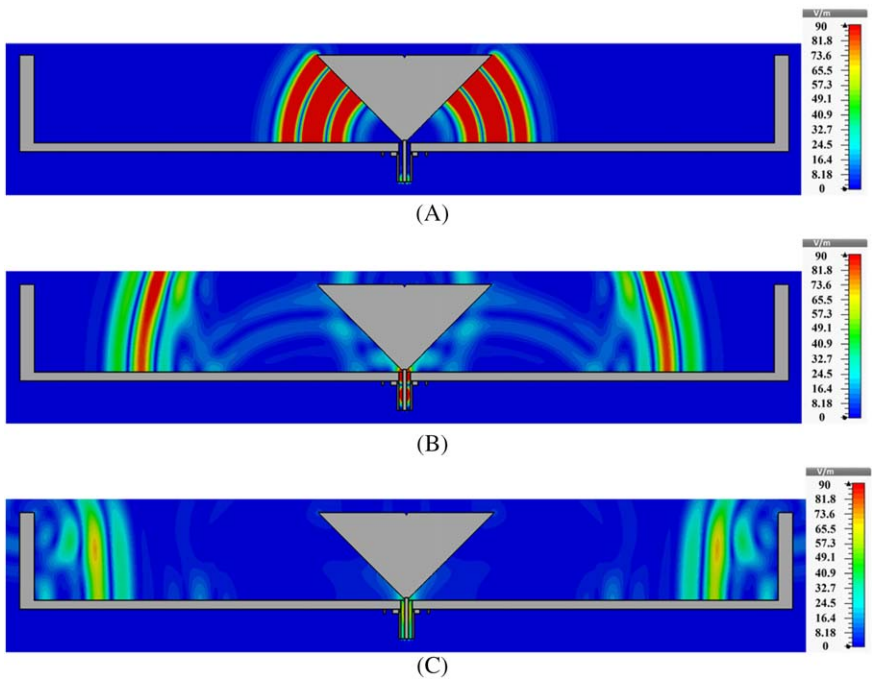

FIGURE 4 Simulated transient electrical field distribution (*xz*-plane) of the mono-cone inside the conventional circular cavity: (A) $t = 0.3$ ns, (B) $t = 0.5$ ns, and (C) $t = 0.7$ ns. [Color figure can be viewed at wileyonlinelibrary.com]

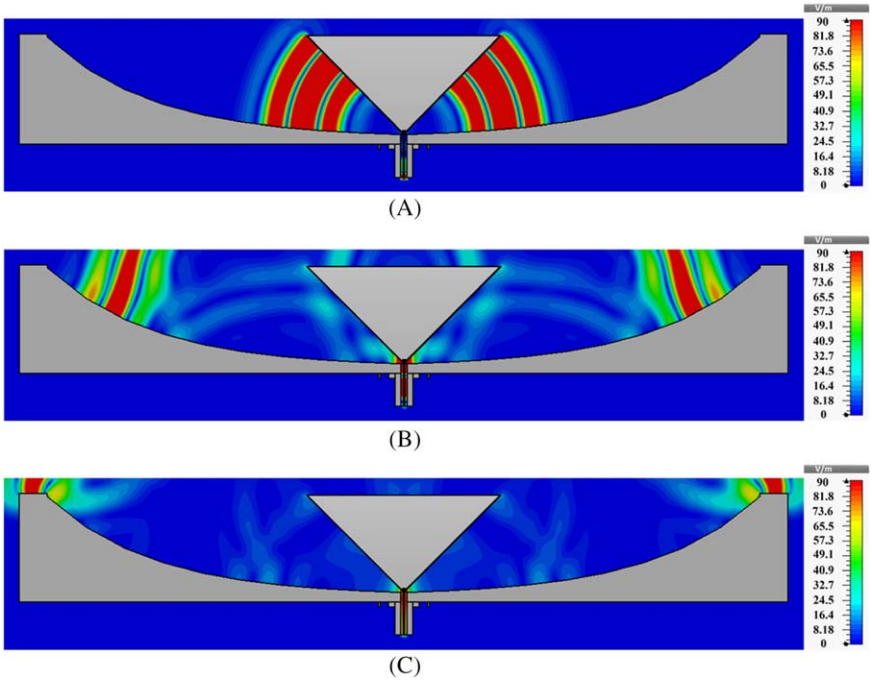

FIGURE 5 Simulated transient electrical field distribution (*xz*-plane) of the mono-cone inside the exponentially tapered cavity: (A) $t = 0.3$ ns, (B) $t = 0.5$ ns, and (C) $t = 0.6$ ns. [Color figure can be viewed at wileyonlinelibrary.com]

the lower limit of the operating frequency at 1 GHz.[11] In step 2, to make the antenna conformal, the mono-cone is placed at the center of a conventional circular cavity, which has a diameter of 224 mm and a depth of 31 mm. In step 3, the profile of the bottom of the cavity is tapered using Equation 1.

Figure 2 shows the simulated return loss characteristics and illustrations of the antenna shape for each step. The designed mono-cone over the flat ground has a broad 10-dB return loss bandwidth from 1.05 GHz to over 15 GHz. However, the return loss characteristic deteriorates when the mono-cone is positioned inside the cavity. Figure 3 shows

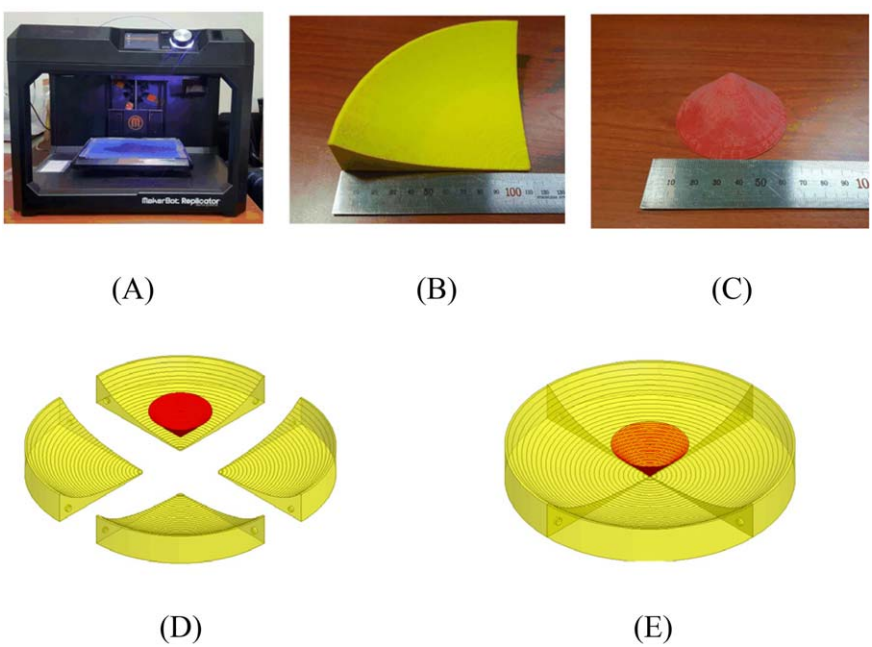

FIGURE 6 Photograph of the printed parts of the antenna: (A) 3D printer, (B) the tapered cavity, (C) the printed mono-cone, (D) dismantled parts, and (E) assembled parts. [Color figure can be viewed at wileyonlinelibrary.com]

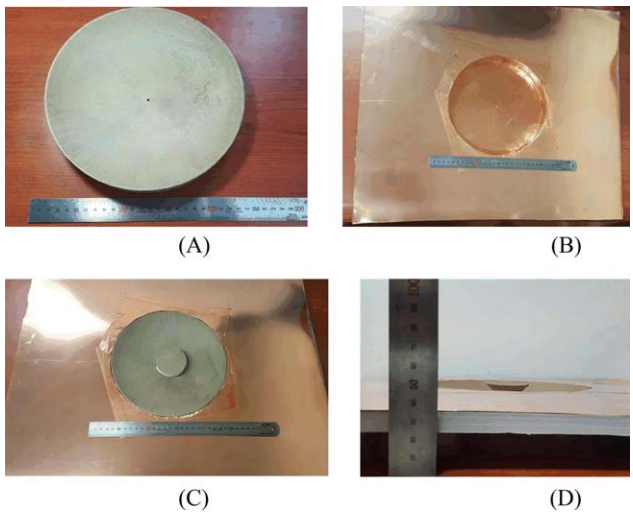

FIGURE 7 Fabrication of the antenna: (A) 3D-printed tapered structure, (B) 3D-printed conventional cavity, (C) top view of the fabricated antenna, and (D) side view of the fabricated antenna. [Color figure can be viewed at wileyonlinelibrary.com]

the comparison between the simulated input resistance and reactance characteristics when the mono-cone is placed over the flat ground and inside the conventional circular cavity. Additionally, for the various profiling factor (B) values shown in Table 1, the simulated input resistance and reactance of the mono-cone inside the exponentially tapered cavity are also shown in Figure 3. The mono-cone inside the conventional circular cavity exhibits higher reactance than that on the flat ground, causing mismatch. As the value of the profiling factor (B) decreases, the mono-cone inside the exponentially tapered cavity has a reactance oscillating with a small ripple, and the resistance approaches 50 Ω so that the antenna operates like the mono-cone on the flat ground.

In order to investigate the functional principle of the exponentially tapered cavity, we compare the transient characteristics of the electrical field propagating in the exponentially tapered cavity and the conventional circular cavity using CST Microwave Studio.[12] Figures 4 and 5 show the simulated transient electrical field distributions inside a conventional circular cavity and the exponentially tapered cavity after a Gaussian pulse is excited. When the mono-cone is placed inside the conventional circular cavity, the electrical field is reflected at the outer region of the cavity. In contrast, the electrical field of the mono-cone inside the exponentially tapered cavity propagates with little reflection at the outer region of the cavity, which causes the antenna to have a high return loss value.

2.3 | Fabrication using a 3D printer

The entire structure was printed using a MakerBot 3D printer whose resolution is 0.1 mm.[13] Figure 4A shows the 3D printer. Due to the limited capacity of the printer, the entire structure was split into 5 pieces. Each piece was printed separately as shown in Figures 4B,C, and they were assembled as shown in Figures 4D,E. Then, the assembled structure was coated with 3 layers of conductive paint, which contains silver particles to produce conducting properties.[14] Figure 6 shows the fabricated antennas.

3 | SIMULATED AND MEASURED RESULTS

Figure 7 shows the photographs of the fabricated antenna. The cavity was fabricated by attaching copper sheets at the outer shell of the 3D-printed conventional cavity. Then, the 3D-printed tapered structure coated with 3 layers of conductive paint was inserted into the conventional cavity. The supporting structure is used to make the mono-cone perpendicularly erect on the tapered structure. The SMA connector was attached to the mono-cone and the bottom of the cavity using a conductive epoxy material instead of soldering.

Figure 8 shows the simulated and measured return loss characteristics of the antenna. The simulated and measured 10-dB return loss bandwidths of the antenna are 22.17 GHz ranging from 1.03 to 23.2 GHz (183%) and 24.4 GHz ranging from 1.3 to 25.7 GHz (180%), respectively, showing that the results are in good agreement. The simulated and measured far-field radiation patterns of the antenna in the *xy*- and *xz*-planes for different frequencies are shown in Figure 9. The measured far-field radiation patterns of the proposed antenna show good agreement with the simulated ones, exhibiting omnidirectional patterns at all frequencies.

Figure 10 shows the simulated and measured peak gains of the proposed antenna. The proposed antenna has some performance degradation in the far-field gain due to the high resistance of the conductive spray and the surface

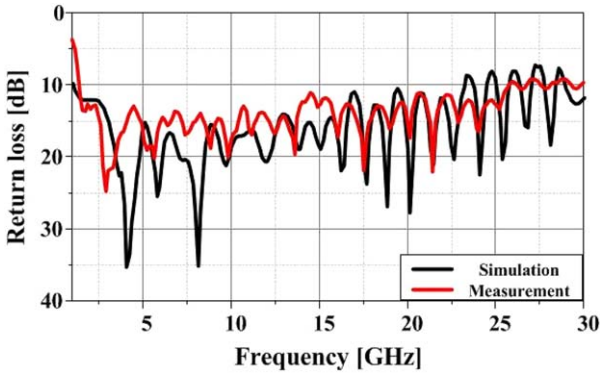

FIGURE 8 Measured and simulated return loss characteristics of the fabricated antenna. [Color figure can be viewed at wileyonlinelibrary.com]

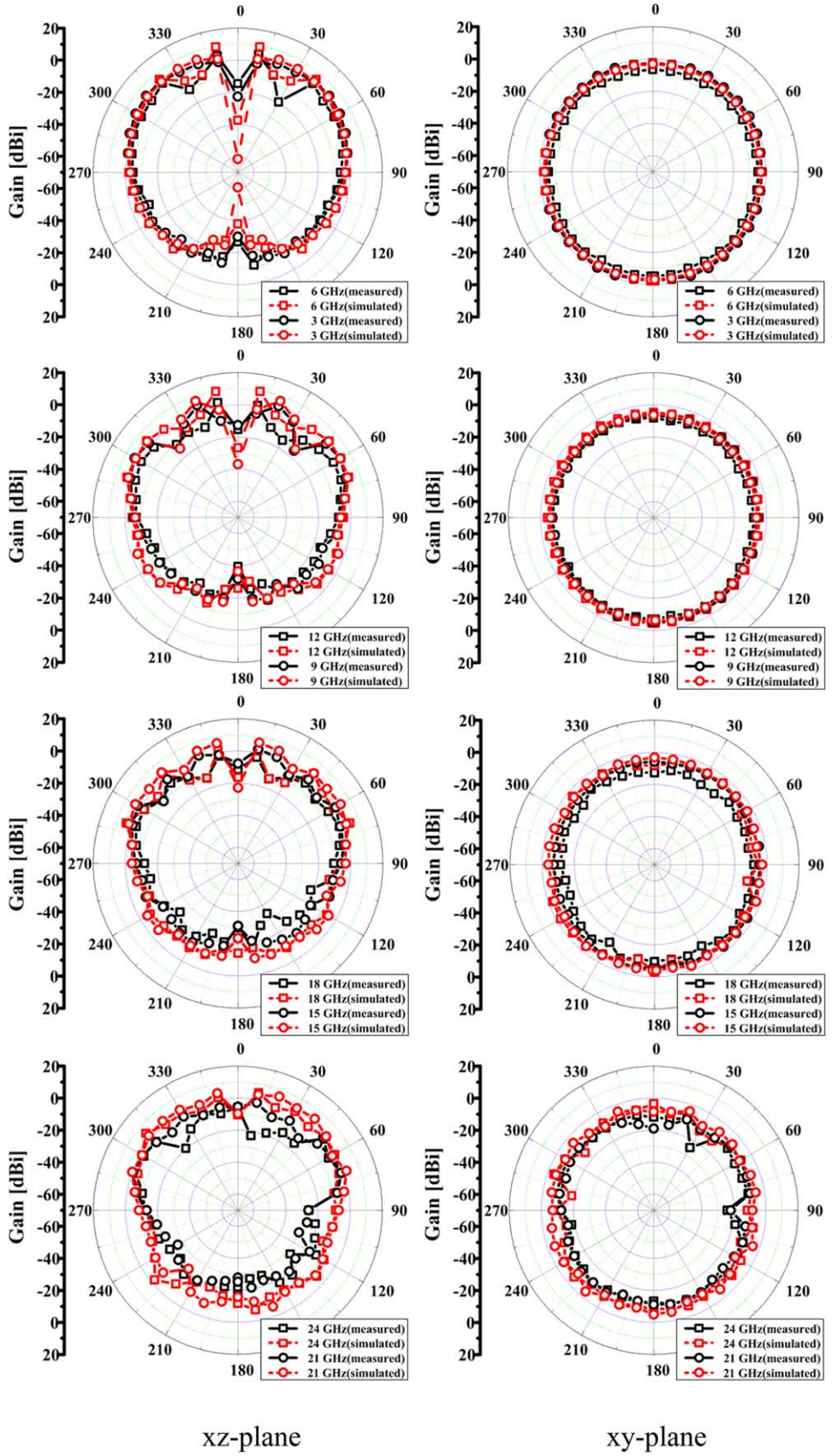

FIGURE 9 Simulated and measured radiation patterns of the proposed antenna in the *xz*- and *xy*-planes at 3, 6, 9, 12, 15, 18, 21, and 24 GHz. [Color figure can be viewed at wileyonlinelibrary.com]

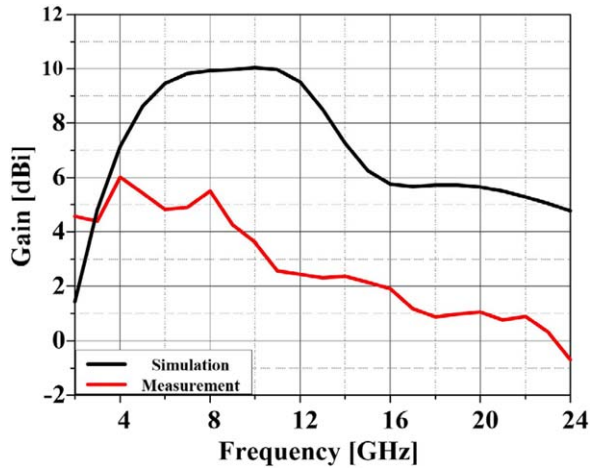

FIGURE 10 Simulated and measured peak gains of the proposed antenna. [Color figure can be viewed at wileyonlinelibrary.com]

roughness.[7,15,16] The measured peak gain of the proposed antenna varies from −0.68 dBi to 5.5 dBi.

4 | CONCLUSION

In this article, a 3D-printed tapered cavity-backed flush-mountable wideband antenna for UAV was proposed. The proposed antenna consists of 3D-printed structures coated with conductive paint. To demonstrate the feasibility of applying 3D printing technology to antenna manufacturing, the return loss and radiation characteristics are simulated and measured. The obtained results show that the antenna has a wide 10-dB return loss bandwidth and monopole-like radiation pattern, verifying the validity of the approach used in this article. Thus, the proposed antenna could be a good candidate for aerial applications and can be utilized directly for UAV.

ACKNOWLEDGMENTS

This work was supported by the research fund of the Signal Intelligence Research Center supervised by the Defense Acquisition Program Administration and Agency for Defense Development of Korea.

ORCID

Seongkyu Lee http://orcid.org/0000-0002-6984-8830

REFERENCES

[1] Valavanis KP, ed. *Advances in Unmanned Aerial Vehicles: State of the Art and the Road to Autonomy*. Springer, New York, NY; 2007.

[2] Sun B-H, Wei Y-F, Zhou S-G, Liu Q-Z. Low-profile and horizontally-polarised antenna for UAV applications. *IET Electron Lett.* 2009;45(22):1106–1107.

[3] Sun L, et al. Dual-band, low-profile, vertically polarized annular ring slot antenna embedded in a small metallic UAV. *Microw Opt Technol Lett.* 2016;58(2):323–328.

[4] Liu Q, et al. A novel broad beamwidth conformal antenna on unmanned aerial vehicle. *IEEE Antennas Wireless Propag Lett.* 2012;11:196–199.

[5] Duangtang P, Mesawad P, Wongsan R. Creating a gain enhancement technique for a conical horn antenna by adding a wire medium structure at the aperture. *KIEES J Electromagn Eng Sci.* 2016;16(2):134–142.

[6] Rufail L, Laurin J. Aircraft cavity-backed nonprotruding wideband antenna. *IEEE Antennas Wireless Propag Lett.* 2012;11:1108–1111.

[7] Hoel KV, Kristoffersen S, Moen J, Holm G, Lande TS. Characterization of a 3D printed wideband waveguide and horn antenna structure embedded in a UAV wing. 2016 10th European Conference on Antennas and Propagation (EuCAP), Davos, 2016, pp. 1–4.

[8] Wu YF, Cheng YJ. Spherical conformal antenna array based on 3D printing framework. 2016 IEEE MTT-S International Microwave Workshop Series on Advanced Materials and Processes for RF and THz Applications (IMWS-AMP), Chengdu, 2016, pp. 1–2.

[9] Rohrdantz B, Rave C, Jacob AF. 3D-printed low-cost, low-loss microwave components up to 40 GHz. 2016 IEEE MTT-S International Microwave Symposium (IMS), San Francisco, CA, 2016, pp. 1–3.

[10] Ansys HFSS. ver. 2015.2, Ansys Corporation, Pittsburgh, PA, 2017.

[11] Johnson RC, Jasik H. *Antenna Engineering Handbook*. 2nd ed. New York: McGraw-Hill; 1984.

[12] CST Corporation, Tech. Rep., CST MWS Ver. 15.0, 2017.

[13] MakerBot Replicator 5th Generation 3D Printer [Online]. Available: http://download.makerbot.com/replicator/MB_Replicator_UserManual.pdf

[14] 842AR—SUPER SHIELD™ SILVER CONDUCTIVE COATING [Online]. Available:http://www.mgchemicals.com/products/emi-and-rfi-shielding/acrylic-conductive-coatings/842ar-super-shield-silver-conductive-coating

[15] Tak J, Kang D-G, Choi J. A lightweight waveguide horn antenna made via 3D printing and conductive spray coating. *Microw Opt Technol Lett.* 2017;59(3):727–729.

[16] Hoel1 KV, Kristoffersen S, Moen J, Kjelgård KG, Lande TS. 3D-printed low-cost, low-loss microwave components up to 40 GHz. 2016 10th European Conference on Antennas and Propagation (EuCAP), Davos, 2016, pp. 1–5.

How to cite this article: Lee S, Jeoung G, Choi J. Three-dimensional-printed tapered cavity-backed flush-mountable wideband antenna for UAV. *Microw Opt Technol Lett*. 2017;59:2975–2981. https://doi.org/10.1002/mop.30863